Periodica Polytechnica Electrical Engineering and Computer Science, 69(3), pp. 318–333, 2025

Multi-objective Site Selection and Capacity Optimization of Distributed PV Energy Storage in Smart Distribution Network Based on Non-cooperative Game

Hongshen Su[1], Tian Zhao[1], Yulong Che[1*], Leijiao Ge[1,2], Xiping Ma[3], Yangyang Zheng[1]

[1] School of Automation and Electrical Engineering, Lanzhou Jiaotong University, 88 Anning West Road, 730070 Lanzhou, China
[2] School of Electrical and Information Engineering, Tianjin University, 92 Weijin Road, 300072 Tianjin, China
[3] State Grid Gansu Electric Power Co., Ltd., Electric Power Research Institute, 249 Wanxin North Road, Anning District, 730070 Lanzhou, Gansu, China
* Corresponding author, e-mail: cylg717@163.com

Received: 10 April 2025, Accepted: 12 August 2025, Published online: 17 September 2025

Abstract

The disordered integration of high-penetration distributed photovoltaics (DPVs) into smart distribution networks has caused critical challenges including transformer reverse overloading and degraded power quality. Strategically deploying grid-level energy storage systems (ESSs) presents an effective solution to address these issues while enhancing operational efficiency and power quality. This paper proposes a non-cooperative game theory-driven optimal siting and sizing method for DPVs and ESSs in smart distribution networks. A tri-objective optimization model is formulated to mitigate grid vulnerability, reduce power losses, and minimize life-cycle carbon emissions of PV generation. To resolve conflicting interests among multiple stakeholders (DPV owners, ESS operators, and grid companies), a non-cooperative game framework with equilibrium strategies is established. An improved multi-objective particle swarm optimization (IMOPSO) algorithm is developed to solve the Nash equilibrium point that maximizes benefits for all participants. Case studies on IEEE 33 bus and IEEE-69 bus distribution systems demonstrate that the proposed method achieves: 2.43% reduction in grid vulnerability index, 4.29% decrease in network losses, and 44.44% reduction in PV life-cycle carbon emissions – all while maintaining voltage quality requirements and realizing Pareto-optimal allocation solutions for multi-stakeholder interests.

Keywords

smart distribution grids, distributed photovoltaics, energy storage, siting, capacity, life cycle carbon emissions, non-cooperative gaming

1 Introduction

With the deepening of global energy transition, the large-scale application of distributed photovoltaic (DPV) and energy storage systems (ESSs) in intelligent distribution networks has become a critical pathway to achieve the "double carbon" goals. As of the end of September 2024, China's PV installed capacity has reached 770 GW, with distributed PV accounting for 44.2%, and the installed capacity of new energy storage projects exceeding 31.39 GW [1, 2]. However, issues such as aggravated line losses and node voltage deviations caused by high-penetration distributed PV access pose severe challenges to the safe and economic operation of distribution networks [3]. Distributed ESSs, with their characteristics of decentralized deployment and flexible regulation, serve as a key means to mitigate the disordered energy flow in distribution networks and enhance PV consumption capacity [4, 5]. How to collaboratively optimize the siting and sizing of distributed PV and energy storage in distribution networks to balance power quality improvement, economic efficiency optimization, and carbon emission reduction goals has become the core issue in current intelligent distribution system planning.

Existing studies have made progress in constructing objective functions and developing solution methods for the optimal siting and sizing of PV-storage systems. Early research primarily focused on economic objectives, such as minimizing investment and operation costs [6, 7]. With the upgrading of low-carbon transition requirements, some scholars have attempted to incorporate carbon emissions into the evaluation system – for example, Li et al. [8] established a life-cycle carbon emission evaluation framework for PV systems. However, existing methods still focus on emission accounting during the operation phase, with

Cite this article as: Su, H., Zhao, T., Che, Y., Ge, L., Ma, X., Zheng, Y. "Multi-objective Site Selection and Capacity Optimization of Distributed PV Energy Storage in Smart Distribution Network Based on Non-cooperative Game", Periodica Polytechnica Electrical Engineering and Computer Science, 69(3), pp. 318–333, 2025. https://doi.org/10.3311/PPee.40676

insufficient tracking of full-chain carbon emissions in manufacturing, decommissioning, and other stages [9, 10].

In terms of power grid reliability, Zheng et al. [7], Shang et al. [11], Li et al. [12] and Yan et al. [13] proposed multi-objective optimization models considering vulnerability indices and network loss characteristics, but a systematic analysis of the coupling relationship among power grid vulnerability, loss characteristics, and life-cycle carbon emissions has not been formed. In terms of solution algorithms, intelligent algorithms such as improved particle swarm optimization have been widely applied to multi-objective optimization [14, 15], but there is a problem of inconsistent evaluation criteria for optimal solutions [16]. Although distributed optimization methods based on non-cooperative games can effectively coordinate the interests of multiple agents [17–19], they have not fully integrated power grid security constraints and life-cycle carbon emission objectives. This makes them difficult to address the goal conflicts among PV prosumers, energy storage operators, and grid operators in modern intelligent distribution systems – specifically, maximizing power generation profits, balancing peak-shaving benefits and capital expenditures, and minimizing system security risks and losses – thus causing the traditional centralized framework to easily fall into a suboptimal solution dilemma.

To address these research gaps, this study constructs a non-cooperative game-driven multi-objective optimization framework, aiming to resolve the uncertainties in energy flow caused by spatiotemporal heterogeneity of PV resources and load volatility, the collaborative optimization needs for grid vulnerability, network loss, and life-cycle carbon emissions, and the decision-making coordination challenges under multi-stakeholder goal conflicts in high-penetration distributed PV distribution networks. The study models the siting and sizing decisions of distributed PV and energy storage as independent gaming agents, achieving multi-agent strategy coordination through Nash equilibrium solutions to break through the interest coordination limitations of traditional centralized optimization. The framework integrates three major objectives – alleviating grid vulnerability, reducing network losses, and minimizing life-cycle carbon emissions of PV power generation – while constructing a multi-dimensional constraint model including power balance, voltage constraints, and energy storage operation characteristics. An improved multi-objective particle swarm optimization (IMOPSO) algorithm is proposed, enhancing solution efficiency through crossover mutation and adaptive weight mechanisms, and integrating the entropy weight-TOPSIS method for comprehensive scheme evaluation combining subjective and objective criteria. Case studies on IEEE-33 [13] and IEEE-69 [15] bus systems verify that the proposed method reduces life-cycle carbon emissions of PV power generation by 44.44%, decreases grid vulnerability by 2.43%, and lowers system network losses by 4.29%, while effectively optimizing energy storage configuration costs. The research findings provide a decision-making tool balancing safety, economy, and low carbon for distribution network planning with high-proportion distributed energy, facilitating efficient planning and operation of new power systems in collaborative scenarios of multiple agents.

The main contributions of this paper are summarized as follows:

1. This study integrates full-chain carbon emissions of photovoltaic (PV) power generation throughout its life cycle with objectives of mitigating grid vulnerability and reducing network losses based on life cycle assessment (LCA) theory, achieving collaborative optimization of distribution network security and low-carbon performance *via* physical constraints.
2. This study addresses the challenge of balancing heterogeneous objectives among PV prosumers, energy storage operators, and grid operators in traditional centralized frameworks. It models PV and energy storage siting/sizing as independent gaming agents, constructs a strategic interaction mechanism based on Nash equilibrium theory, and achieves Pareto-optimal coordination of multi-agent strategies to resolve suboptimal solutions caused by insufficient interest alignment in conventional approaches.
3. This study addresses the defects of poor solution set quality and single evaluation criteria in existing multi-objective algorithms. It introduces crossover mutation and adaptive weight mechanisms into the traditional multi-objective particle swarm optimization (MOPSO) algorithm, and constructs a comprehensive evaluation system by combining the entropy weight-TOPSIS method. Case studies show that this method significantly optimizes multiple indicators, providing a replicable scheme for intelligent distribution network planning.

The remainder of this paper is organized as follows: Section 2 details the life-cycle carbon emission assessment of PV generation, integrating material manufacturing to decommissioning phases. Section 3 formulates the multi-objective optimization model for distributed PV and

ESSs, incorporating grid vulnerability mitigation, network loss reduction, and life-cycle carbon emission minimization. Section 4 develops a non-cooperative game-theoretic framework to solve the multi-objective model, establishing strategic interaction mechanisms among stakeholders based on Nash equilibrium theory. Section 5 presents case studies using IEEE standard test systems [13, 15], including comparative analyses and sensitivity evaluations. Finally, Section 6 summarizes the conclusions and future research directions.

2 Carbon emissions during the life cycle of PV power generation

The life-cycle carbon emissions of PV systems (from manufacturing to recycling) inform the optimal siting and sizing of distributed PV and ESSs, reducing cumulative emissions while balancing resource efficiency with grid stability.

Life-cycle carbon emissions of PV generation have been widely used in power supply chains to track carbon footprints. The full life cycle carbon emissions of PV systems encompass manufacturing, transportation, installation, operation, and decommissioning phases (as illustrated in Fig. 1). During planning, it is critical to holistically evaluate regional PV resource endowments (e.g., solar irradiance levels), spatial availability (e.g., rooftop/wasteland suitability), and supply chain carbon footprints, thereby reducing the overall carbon emission intensity through optimal siting strategies [20]. A full life cycle emission (LCE) analysis of PV generation is integrated into sustainable development goal (SDG) planning processes. This integration achieves dual objectives: ensuring operational compliance and minimizing carbon emissions in distributed PV and energy storage siting and sizing optimization. This approach not only facilitates cost optimization but also contributes to life cycle carbon footprint reduction across the entire PV deployment process.

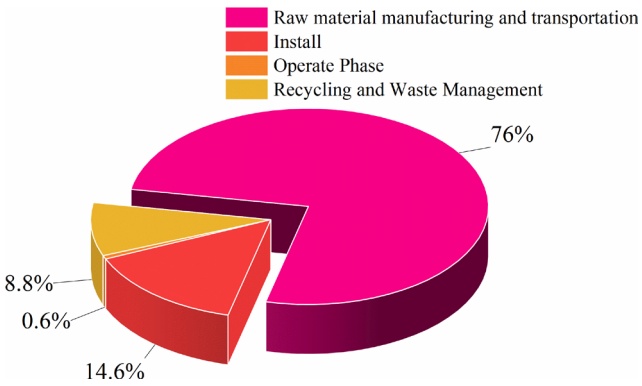

Fig. 1 Distribution of carbon emissions at different stages of the life cycle of PV power generation

The indirect carbon emissions associated with PV manufacturing is shown in Eq. (1):

$$C_{pro,id}^{\mathrm{PV}} = P_{all}^{\mathrm{PV}} \sum_{i=1}^{n} cBf, \tag{1}$$

where P_{all}^{PV} is the total PV power output; c is the carbon emission factor per unit of electricity; n is the number of distinct generating units; B is the electricity consumption in PV manufacturing and f is the PV system influence coefficient.

The life cycle greenhouse gas emissions from PV product transport are shown in Eq. (2):

$$C_{tra}^{\mathrm{PV}} = 20\%\left(C_{pro,de}^{\mathrm{PV}} + C_{pro,id}^{\mathrm{PV}}\right), \tag{2}$$

where $C_{pro,de}^{\mathrm{PV}}$ is the direct carbon emissions during the PV production process. The carbon emissions in the PV recycling phase consist of multiple components, including emissions from raw material reprocessing, constraints related to the maximum installed capacity of recycling facilities, and technology-specific emission factors (Eq. (3)):

$$C_{re}^{\mathrm{PV}} = \varpi_1^{\mathrm{PV}} \zeta^{\mathrm{PV}} P_{in,\max}^{\mathrm{PV}} + \varpi_2^{\mathrm{PV}} \left(1-\zeta^{\mathrm{PV}}\right) P_{in,\max}^{\mathrm{PV}}, \tag{3}$$

where ϖ_1^{PV} and ϖ_2^{PV} are the carbon emission factors of recyclable and non-recyclable PV components, respectively; ζ^{PV} is the PV recycling rate and $P_{in,\max}^{\mathrm{PV}}$ is the maximum installed capacity of the PV system.

The life cycle carbon emissions of PV power generation [9] are shown in Eq. (4):

$$C_{\mathrm{LCA}}^{\mathrm{PV}} = C_{pro,de}^{\mathrm{PV}} + C_{pro,id}^{\mathrm{PV}} + C_{tra}^{\mathrm{PV}} + C_{re}^{\mathrm{PV}}. \tag{4}$$

3 Equations

The proposed multi-objective optimization model for distributed PV and ESS incorporates three critical objectives: grid vulnerability mitigation (assessed *via* voltage deviation metrics and Gini coefficient-based uniformity analysis)), network loss minimization, and life-cycle carbon emission reduction. It defines constraints including power balance, node voltage limits, and energy storage operational boundaries (power/energy capacity limits, state-of-charge (SoC) constraints) to ensure system stability and equipment longevity. This framework facilitates collaborative planning of PV-storage deployment while balancing technical, economic, and environmental trade-offs in smart distribution networks.

3.1 Objective function

By integrating the power grid vulnerability metric x_1, active power loss x_2, and life cycle carbon emissions metric x_3,

the multi-objective optimization function is formulated as follows (Eq. (5)):

$$X_r = \min\left(x_1, x_2, x_3\right). \tag{5}$$

3.1.1 Overall vulnerability index

Distributed energy storage systems (DESS) exhibits two essential operational characteristics: decentralized deployment architecture and bidirectional power flow controllability. These technical attributes enable effective mitigation of stochastic power fluctuations and disordered energy flow patterns in modern distribution networks. Critical vulnerable nodes face the risk of cascading failure propagation under contingency conditions. Line component failures triggered by system disturbances or external disruptions may induce widespread blackout events. Node vulnerability assessment employs a voltage deviation index (VDI) which quantifies operational state stability by comparing nodal voltage magnitudes against reference thresholds (Eq. (6)):

$$V_{i,t} = \frac{\left|U_{i,t}^{*} - 1\right|}{\Delta U_{\max}}, \tag{6}$$

where $U_{i,t}^{*}$ represents the per unit voltage at node i during time period t and $\Delta U_{\max}$ denotes the maximum allowable voltage deviation.

Based on the power grid vulnerability index defined in Eq. (6), the aggregated vulnerability index can be derived as follows (Eq. (7)):

$$V_t^{ent} = \frac{1}{N}\sum_{i=1}^{N}\frac{V_{i,t} - V_{t,\min}}{V_{t,\max} - V_{t,\min}}, \tag{7}$$

where N is the total number of nodes in the distribution network, $V_{t,\max}$ and $V_{t,\min}$ denotes the maximum and minimum values of the nodal vulnerability index during time period t, respectively.

The structural homogeneity of a distribution network significantly influences its vulnerability. An uneven distribution of nodal vulnerabilities may lead to cascading failures within the grid if a voltage collapse occurs at any single node. Therefore, relying solely on system-level vulnerability assessments is insufficient for comprehensive risk evaluation. This paper proposes the Gini coefficient as a metric V_t^{equ} to quantify the uniformity of vulnerability distribution in distribution networks (Eq. (8)):

$$V_t^{equ} = 1 - \frac{1}{N}\left(2\sum_{i=1}^{N-1} H_{i,t} + 1\right), \tag{8}$$

where $H_{i,t}$ represents the ratio of the cumulative sum of vulnerability indices of the first i nodes (sorted in ascending order) to the total sum of all nodal vulnerability indices during time period t.

The comprehensive vulnerability index (V^{com}) is proposed to holistically evaluate the vulnerability of distribution networks. As formulated in Eq. (8), the V^{com} integrates weighted structural and operational vulnerability components, where the weighting coefficients ω_1 and ω_2 are both set to 0.5. The V^{com} is bounded within the range of [0,1], with higher values indicating diminished disturbance resistance capability of the distribution network and reduced risk resilience of the grid system [13]:

$$x_1 = V^{com} = \frac{1}{T}\sum_{t=1}^{T}\omega_1 V_t^{ent} + \omega_2 V_t^{equ}. \tag{9}$$

3.1.2 Network loss

The daily network loss is calculated using Eq. (10):

$$x_2 = \sum_{t=1}^{24}\sum_{j\in M_L}\left[G_{ij}\left(U_{i,t}^2 + U_{j,t}^2 - 2U_{i,t}U_{j,t}\cos\delta_{ij,t}\right)\right], \tag{10}$$

where M_L represents all the branches in the network; G_{ij} stands for the set of conductances at nodes i and j; $U_{i,t}$ and $U_{j,t}$ are the voltages at nodes i and j at time t and $\delta_{ij,t}$ is the phase-angle difference between the start-node i and the end-node j of the branch at time t.

3.1.3 Carbon emission indicators for the life cycle of PV power generation

The carbon emission indicator x_3 for the LCA of PV power generation where distributed PV is integrated into a smart distribution network is adopted as the third objective function for optimization, and the life cycle carbon emissions of PV power generation can be obtained from Eq. (4):

$$x_3 = C_{\mathrm{LCA}}^{\mathrm{PV}}. \tag{11}$$

3.2 Constraints

When determining the location and capacity configuration of distributed PV and ESS in a smart distribution network, not only must the fundamental operational constraints of the system be fully considered, such as power balance and node voltage, but also the power and energy balance of the ESS and strategies to mitigate energy fluctuations should be comprehensively evaluated [13].

3.2.1 Power balance constraints

The power balance constraint formula is used as (Eq. (12)):

$$P_s = \sum_{i=1}^{n_{bus}} P_{li} - \sum_{j=1}^{n_D} P_{Dj} - \sum_{k=1}^{n_s} P_{ek}, \tag{12}$$

where P_s denotes the input power of the power grid; P_{li} represents the load power at node i at time t; P_{Dj} is the output power of the j-th distributed PV system at time t; P_e refers to the output power of the k-th ESS at time t (positive during discharge) and n_D represents the total number of distributed PV systems.

3.2.2 Node voltage constraint

The node voltage constraint formula is used as (Eq. (13)):

$$v_{\min} \le v_{ij} \le v_{\max}, \tag{13}$$

where $v_{\min}$ and $v_{\max}$ represent the lower and upper limits of the system node voltage, respectively.

3.2.3 Energy storage power constraint

The energy storage power constraint formula is used as (Eq. (14)):

$$P_{s_{\min}} \le P_s \le P_{s_{\max}}, \tag{14}$$

where $P_{s_{\min}}, P_{s_{\max}}$ represent the lower and upper limits of the ESS power, respectively.

3.2.4 Energy storage energy balance constraint

The Energy storage energy balance constraint formula is used as (Eq. (15)):

$$\begin{cases} p_{st,k}^{\min} \le p_{st,k}(t) \le p_{st,k}^{\max} \\ E_{st,k}(t) = E_{store,k}(t-1)(1-\delta) \\ +p_{st,k}(t)\eta_c \Delta t\left(p_{st,k}(t) \le 0\right) \\ E_{st,k}(t) = E_{st,k}(t-1)(1-\delta) \\ -\dfrac{p_{st,k}(t)}{\eta_d}\Delta t\left(p_{st,k}(t) > 0\right) \\ 0.2 \le \mathrm{SOC}_k(t) \le 0.9\left(\mathrm{SOC}_k(0) = 0.5\right) \\ \sum\limits_{t=1}^{T}\left[p_{st,k}(t)a_1\eta_c + p_{st,k}(t)\dfrac{a_2}{\eta_d}\right]\Delta t = 0 \end{cases}, \tag{15}$$

where $p_{st,k}^{\min}$, $p_{st,k}^{\max}$ denote the upper charging power limit and lower discharging power limit of the k-th energy storage unit, respectively; $E_{st,k}(t)$ represents the capacity of energy storage k at time t; δ indicates the self-discharge rate; η_c and η_d are the charging efficiency and discharging efficiency of the ESS and $\mathrm{SOC}_j(t)$ notes the state of charge of energy storage at time t. To prevent lifespan degradation caused by overcharging or over discharging, its value is constrained to the range 0.2–0.9, and it is initialized and terminated at 0.5 at the start and end of each operational cycle, respectively.

In Eq. (15) a_1 and a_2 are binary charging/discharging state variables:

- when the power $p_{st,k}(t) \le 0$ (charging mode), $a_1 = 1$, $a_2 = 0$;
- when $p_{st,k}(t) > 0$, (discharging mode), $a_1 = 0$, $a_2 = 1$.

4 Solution strategy for multi-objective optimization model driven by non-cooperative game theory

PV prosumers in SDNs prioritize generation revenue maximization. This economic driver incentivizes high-capacity PV installations at network nodes with optimal solar irradiance conditions. However, this strategy risks exacerbating local voltage violations due to intermittent power injection. Energy storage operators seek to maximize the net benefit of peak-shaving revenue minus investment costs, typically deploying storage systems at nodes with significant load fluctuations. While effective for load balancing, their charging-discharging behaviors may inadvertently increase network losses. Grid operators, prioritizing minimization of comprehensive costs (including network losses, system vulnerability, and carbon emissions), must regulate the location and capacity of PV and energy storage deployments to balance these conflicting objectives.

4.1 Game elements

A non-cooperative game-theoretic framework is employed to model this multi-agent interaction. Through iterative optimization of individual strategies, all stakeholders are driven to converge to a Nash equilibrium, where no party can unilaterally improve its payoff. This equilibrium represents a globally optimal compromise that balances economic incentives with grid stability and efficiency.

SDN planning inherently involves game-theoretic dynamics. Strategic interactions between PV systems and ESS emerge during siting-sizing optimization processes, driving the system toward competitive equilibrium states. The non-cooperative game-theoretic strategies between PV and ESS, driven by their conflicting operational objectives, are formulated as follows:

$$\boldsymbol{R} = \{\boldsymbol{G}; \boldsymbol{S}; \boldsymbol{X}\}. \tag{16}$$

The specific description is as follows:

- Player G: in the game-theoretic framework, each participant with independent decision-making authority is termed a player (denoted as G). Within smart distribution networks, the players are categorized as distributed PV systems ($\boldsymbol{G}_{\mathbf{PV}}$) and ESS ($\boldsymbol{G}_{\mathbf{ESS}}$). These players collectively form the set of strategic agents $\boldsymbol{G} = \{\boldsymbol{G}_{\mathbf{PV}}, \boldsymbol{G}_{\mathbf{ESS}}\}$.

- Strategy set S: in game-theoretic interactions, the feasible strategies adopted by players during decision-making are defined as their actionable plans. In this context, the strategies for PV ($\boldsymbol{S}_{\mathbf{PV}}$) and energy storage ($\boldsymbol{S}_{\mathbf{ESS}}$) systems involve their siting locations and capacity allocations. The strategy set S is formalized as: $\boldsymbol{S} = \{\boldsymbol{S}_{\mathbf{PV}}, \boldsymbol{S}_{\mathbf{ESS}}\}$.
- Payoff X: the payoff function quantifies the benefits obtained by both players during their interactive decision-making processes and is utilized to adjust their subsequent strategies. The mathematical formulation is detailed in Eq. (17):

$$\boldsymbol{X} = \begin{cases} \boldsymbol{X}_{\mathbf{PV}}\left(\boldsymbol{S}_{\mathbf{PV}}, \boldsymbol{S}_{\mathbf{ESS}}\right) \\ \boldsymbol{X}_{\mathbf{ESS}}\left(\boldsymbol{S}_{\mathbf{PV}}, \boldsymbol{S}_{\mathbf{ESS}}\right) \end{cases}, \tag{17}$$

4.2 Existence of Nash equilibrium solutions

All participants aim to maximize $\boldsymbol{X}$. Each participant selects its optimal siting and sizing strategy $\boldsymbol{S}$ based on the strategies chosen by other participants. We define the proposed non-cooperative game as $\boldsymbol{R} = \{\boldsymbol{G}; \boldsymbol{S}; \boldsymbol{X}\}$, where $\boldsymbol{G}$ denotes the set of participants, $\boldsymbol{S}$ is the strategy space, and $\boldsymbol{X}$ represents the payoff function. The strategy vector $\boldsymbol{S}^* = \left(\boldsymbol{S}^*_{\mathbf{PV}}, \boldsymbol{S}^*_{\mathbf{ESS}}\right)$, constitutes a Nash equilibrium if and only if: for every participant, $\boldsymbol{X}^*\left(\boldsymbol{S}^*\right) \geq \boldsymbol{X}\left(\boldsymbol{S}'_{\mathbf{PV}}, \boldsymbol{S}'_{\mathbf{ESS}}\right)$ holds for all $\boldsymbol{S}' = \left(\boldsymbol{S}'_{\mathbf{PV}}, \boldsymbol{S}'_{\mathbf{ESS}}\right) \in \boldsymbol{S}$, where $\boldsymbol{X}(\boldsymbol{S}^*)$ is the payoff at equilibrium, and $\boldsymbol{X}\left(\boldsymbol{S}'_{\mathbf{PV}}, \boldsymbol{S}'_{\mathbf{ESS}}\right)$ is the payoff when the current participant deviates while others maintain their strategies.

According to the Nash equilibrium existence theorem, for a game with N players, if the pure strategy set S_i of each player i is a non-empty, compact, and convex subset of a Euclidean space, and the payoff function X_i^* is continuous and quasi-concave with respect to S_i, then the game admits at least one pure-strategy Nash equilibrium.

Hence, to prove the existence of a Nash equilibrium in the proposed non-cooperative game model, it is necessary to verify that the strategy set S of electricity-selling strategies for all participants is a non-empty, compact, and convex subset, and that the corresponding payoff function is a continuous and quasi-concave function.

4.2.1 Prove that S is a non-empty compact convex subset

S denotes the interval of each participant's strategies spanning from the minimum to maximum siting capacities, where $S = \{S_{\mathrm{PV}}, S_{\mathrm{ESS}}\}$ constitutes a compact convex subset; moreover, a corresponding strategy necessarily exists for each participant when engaging in electricity trading.

4.2.2 Prove that the profit function X is concave

From Eq. (17), the payoff function is linear. According to the Nash equilibrium existence theorem, it suffices to demonstrate that the utility function X is quasi-concave with respect to the strategy set S, which ensures the existence of pure-strategy Nash equilibria in the proposed non-cooperative game model. When S is a known strategy set, X is linear in S; as linear functions are inherently concave (and thus quasi-concave), the region-based operation optimization model under the non-cooperative game framework therefore admits a set of pure-strategy Nash equilibria.

4.3 Solving algorithm

This study proposes a non-cooperative game-driven equilibrium strategy under heterogeneous stakeholder structures. An enhanced MOPSO algorithm is used to derive the strategy. The methodology comprises three key steps:

1. Encoding of decision variables: the locations and capacity configurations of PV systems and the ESS are encoded into the optimization framework.
2. Algorithm enhancement: the conventional MOPSO algorithm is improved by integrating crossover-mutation operations and adaptive weighting mechanisms to enhance convergence and diversity.
3. Multi-objective optimization: this study employs an enhanced MOPSO algorithm to iteratively optimize the siting and capacity allocation for all game participants. The approach leverages equilibrium strategies derived from a non-cooperative game model to balance conflicting objectives, including economic benefits, grid stability, and operational constraints.

4.3.1 Encoding

During the optimization process, the locations and capacities of PV systems and ESS are encoded as decision variables, with the initial capacity of distributed ESS also being incorporated into the encoding framework.

$$\begin{cases} \boldsymbol{S}_{\mathbf{PV}} = \left[c_1, c_2, \ldots, c_{N'}, d_1, \ldots, d_{N'}\right] \\ \boldsymbol{S}_{\mathbf{ESS}} = \left[a_1, a_2, \ldots, a_{M'}, b_1, \ldots, b_{M'}, \ldots, b_{e\cdot M'+g}, \ldots, b_{t\cdot M'}\right] \end{cases}, \tag{18}$$

where N' is the number of PV systems; $c_{N'}$ denotes the grid connection location of the N' distributed PV system, which is subject to rounding operation; $d_{N'}$ is the rated capacity of the N' distributed PV system; M' is the number of distributed ESS denotes the grid connection location of the M' ESS, which is subject to rounding operation;

$b_{e\cdot M'+g}$ represents the real power of the *g*-th ESS at time (*e*+1) and *t* is the time index.

To ensure the energy balance of the ESS, it is necessary to adjust the power of the *g*-th ESS at time *t*:

$$b_{(T-1)e\cdot M'+g} = -\sum_{j=1}^{t-1} b_{(e-1)e\cdot M'+g}. \tag{19}$$

4.3.2 Improving multi objective particle swarm optimization algorithm

In the MOPSO algorithm, crossover and mutation operations are performed on particles' position vectors [21]. The entropy-weighted TOPSIS method is incorporated to enable comprehensive subjective and objective evaluation [22]. This approach aims to enhance population diversity and improve the convergence performance of the algorithm.

In the particle swarm optimization algorithm, each particle represents a candidate solution. The optimization mechanism dynamically updates its position in *d*-dimensional solution space through dual solution guidance mechanisms. This iterative process progressively converges toward global optima [23]. The update strategies for velocity and position are described by Eqs. (20) and (21), respectively:

$$v_{id}^{(k+1)} = wv_{id}^{(k)} + c_1 r_1 \left(p_{id}^{(k)} - x_{id}^{(k)}\right) + c_2 r_2 \left(g_d^{(k)} - x_{id}^{(k)}\right), \tag{20}$$

$$x_{id}^{(k+1)} = x_{id}^{(k)} + v_{id}^{(k+1)}. \tag{21}$$

Adaptive inertia weight

The difference $X_i^{(k)}$ between the *i*-th particle and the global optimal solution of the population at the *k*-th iteration can be calculated using Eqs. (22) and (23):

$$X_i^{(k)} = \frac{1}{x_{\max} - x_{\min}} \frac{1}{D} \sum_{d=1}^{D} \left| g_d^{(k)} - x_{id}^{(k)} \right|, \tag{22}$$

$$w_i^{(k)} = w_{start} - \left(w_{start} - w_{end}\right)\left(X_i^{(k)} - 1\right)^2, \tag{23}$$

where *D* is the dimension of the solution space; $w_i^{(k)}$ is the inertia weight of the *i*-th particle at time *k*; w_{start} and w_{end} denote the initial and final values of the inertia weight; $x_{\max}$ and $x_{\min}$ represent the maximum and minimum values of the particle's velocity variable.

Cross mutation operation

The PSO algorithm is prone to local optima during iterations. To enhance population diversity, crossover and mutation operations from genetic algorithms were incorporated into PSO, improving the particles' position vectors. Based on this, a novel approach was proposed that utilizes the difference vector $\boldsymbol{X}$ between the particle's position vector and the global optimum to perform crossover and mutation operations.

4.3.3 Solution process

The specific steps of the game-theoretic improved PSO algorithm are as follows:

1. Step 1: under capacity constraints, initialize the capabilities of each participant. Each participant's strategy *S* is initialized.
2. Step 2: input system-related parameters and determine the global optimal solution using the entropy-weighted TOPSIS method.
3. Step 3: for siting and sizing of each participant, solve using the improved MOPSO algorithm. Based on the concept of Nash equilibrium, each participant aims to maximize their total profit under the (p−1)-th strategy to derive their optimal solution for the *p*-th siting and sizing plan. The mathematical expression for the optimal siting and sizing plan of each game participant in the *p*-th round is shown in Eq. (24):

$$\begin{cases} \boldsymbol{S}_{\mathbf{PV},p} = \arg\max_{\boldsymbol{S}_{\mathbf{PV},p}} \left(\boldsymbol{S}_{\mathbf{PV},p}, \boldsymbol{S}_{\mathbf{ESS},p-1}\right) \\ \boldsymbol{S}_{\mathbf{ESS},p} = \arg\max_{\boldsymbol{S}_{\mathbf{ESS},p}} \left(\boldsymbol{S}_{\mathbf{ESS},p}, \boldsymbol{S}_{\mathbf{PV},p-1}\right) \end{cases}. \tag{24}$$

4. Step 4: determine whether a Nash equilibrium point has been identified. If two consecutive strategies are identical (i.e., the Nash equilibrium point is derived from Eq. (25)), each participant selects an optimal location based on their strategy and calculates their corresponding profit. Otherwise, return to Step 3:

$$\left(\boldsymbol{S}_{\mathbf{PV}}^*, \boldsymbol{S}_{\mathbf{ESS}}^*\right) = \left(\boldsymbol{S}_{\mathbf{PV},p}, \boldsymbol{S}_{\mathbf{ESS},p}\right) = \left(\boldsymbol{S}_{\mathbf{PV},p-1}, \boldsymbol{S}_{\mathbf{ESS},p-1}\right). \tag{25}$$

5. Step 5: output the Nash equilibrium point $\left(\boldsymbol{S}_{\mathbf{PV}}^*, \boldsymbol{S}_{\mathbf{ESS}}^*\right)$ and the profit function $\boldsymbol{X}$. The solution flowchart for the optimization model of distributed PV and energy storage integration into smart distribution grids, covering siting and sizing, is presented in Fig. 2.

5 Example analysis

5.1 IEEE-33 distribution network system

5.1.1 Data input

To validate the rationality of the proposed method, the IEEE-33 distribution network system was adopted as a case study. The distributed PV system can be integrated at nodes 2 to 33, with 2 units installed at 2 MW each. The total grid load is 3715 + j2300 kVA, operating at 12.66 kV, and the allowable node voltage range is 0.9–1.1 p.u. The ESS can be integrated at nodes 2 to 33, with 2 units

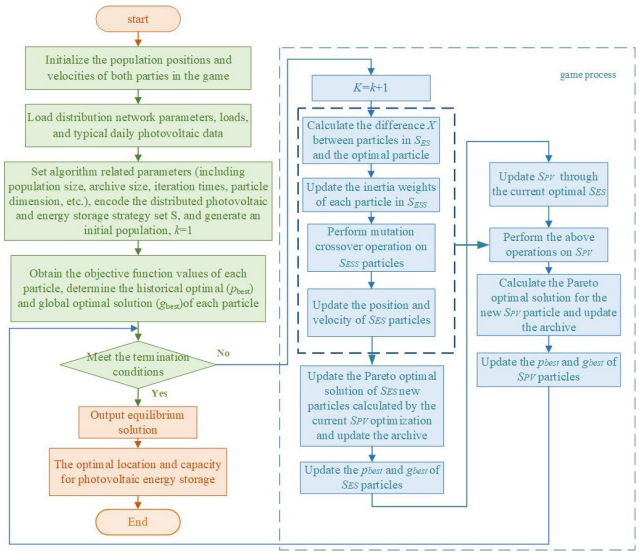

Fig. 2 Distribution network distributed PV and energy storage location and capacity solving process

installed at 2 MW each. Typical daily load and distributed PV output curves are provided in Wu et al. [14], as shown in Fig. 3. Differences in PV resource endowments among nodes 2–33 are represented by equivalent irradiance intensity weights. Supply chain carbon footprint data are referenced from regional grid carbon emission factors, and transportation distances are converted based on the geographical locations of nodes relative to the regional logistics center.

5.1.2 Scene setting

Given the large scale of the optimization solution set, the paper lists the top three Pareto optimal solutions in descending order of weighted indicators. To validate the proposed algorithm's correctness, five distinct scenarios

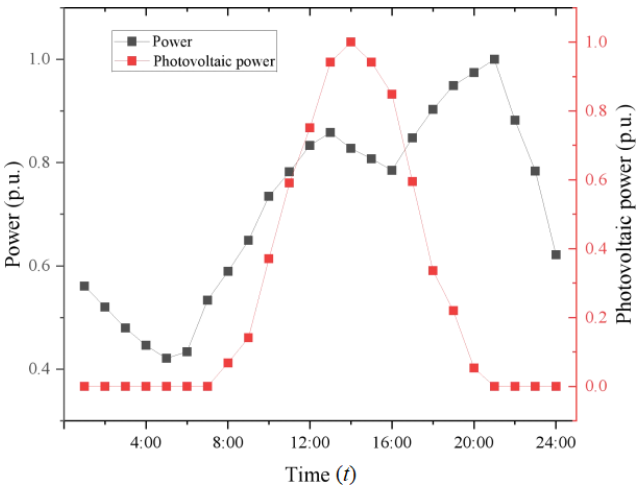

Fig. 3 Daily load and distributed PV output curves

were designed. These scenarios were subjected to comparative analysis under identical constraints:

1. Scenario 1: without energy storage integration, solving for grid vulnerability, network loss, and life-cycle carbon emissions of PV power generation.
2. Scenario 2: incorporating distributed PV and energy storage, the model aims to minimize network loss and PV life-cycle carbon emissions while excluding grid vulnerability.
3. Scenario 3: incorporating distributed PV and energy storage, the model targets minimizing grid vulnerability and network loss while excluding PV life-cycle carbon emissions.
4. Scenario 4: incorporating distributed PV and energy storage, the model uses a multi-objective optimization framework integrating grid vulnerability, network loss, and PV life-cycle carbon emissions, with a traditional MOPSO algorithm employed for siting and sizing of distributed PV and energy storage.
5. Scenario 5: incorporating distributed PV and energy storage, the model adopts a multi-objective optimization framework integrating grid vulnerability, network loss, and PV life-cycle carbon emissions, with a non-cooperative game-driven improved MOPSO algorithm utilized for siting and sizing of distributed PV and energy storage.

5.1.3 Result analysis

Among these, Scenario 5 represents the method proposed in this paper. Scenario 1 is calculated by choosing end-nodes and without deploying energy storage. Scenarios 2 and 3 are contrasted with Scenario 5 by omitting one objective each. Scenario 4 is used for comparison with the method in Scenario 5. Table 1 presents the optimization results for the IEEE-33 bus system, with the sitting outcomes shown in Fig. 4. As indicated in Table 1, compared to Scenario 1, Scenario 5 achieves reductions in all three objective functions: the grid vulnerability index decreased by 2.43%, network loss was reduced by 4.29%, and the life-cycle carbon emissions of PV power generation decrease by 44.44%. Scenario 5 also demonstrated improvements in all indicators compared to the other four scenarios to varying degrees. Scenarios 2 and 3 showed marginal system improvements and exhibited slower convergence speeds compared to Scenario 5. Table 2 [13, 17] shows that the previous research methods have certain advantages.

Table 1 Performance comparison of different scenarios of IEEE-33 bus

Scenario	PV access location and capacity/MW	Energy storage access location and capacity/MW	x_1	x_2	x_3
1	22(2) 18(2)	–	0.3248	1.7810	240000
2	11(1.4842) 15(1.6617)	14(1.7432) 30(1.9038)	0.3206	2.024	188750
	25(1.2247) 33(1.8878)	8(1.3733) 13(1.329)	0.3318	1.9411	186750
	5(1.1541) 9(0.5241)	18(1.8622) 33(1.3013)	0.3040	2.2704	120490
	Average value		0.3188	2.0785	165330
3	31(1.569) 26(1.4232)	31(1.2462) 30(1.3790)	0.3133	1.733	179530
	29(1.6331) 17(1.9906)	24(1.8290) 25(1.4207)	0.3148	1.7426	217420
	12(0.5874) 11(1.1574)	30(1.7076) 8(1.3227)	0.3244	1.7994	104960
	Average value		0.3175	1.7583	167303
4	15(1.7732) 29(1.6078)	10(1.5388) 26(1.5908)	0.3188	1.7308	202850
	27(1.0597) 7(1.3308)	3(1.8332) 32(1.9887)	0.3118	1.7171	143430
	13(0.7019) 23(1.7606)	4(1.5289) 8(1.8885)	0.3221	1.7706	157750
	Average value		0.3176	1.7395	168010
5	32(1.9972) 10(0.6959)	3(1.4906) 31(1.0457)	0.3141	1.7096	161590
	16(0.8885) 32(0.9896)	3(1.9619) 10(1.3532)	0.3182	1.6936	112680
	26(1.0230) 28(1.2389)	28(1.4159) 19(1.1622)	0.3183	1.7114	125720
	Average value		0.3169	1.7048	133330

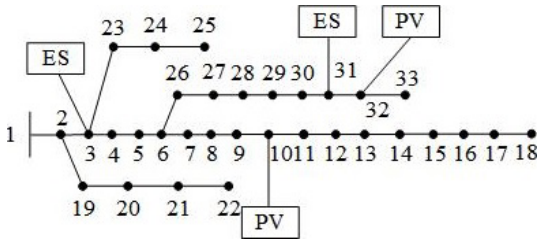

Fig. 4 IEEE-33 bus sitting results

Table 2 Data comparison: quantitative verification of IEEE-33 bus

Evaluating indicator	The research method	Method of Yan et al. [13]	Method of Abuduwayiti et al. [17]
x_1	0.3169	0.3201	0.3187
x_2	1.7048	1.9234	1.8762
x_3	133330	150800	143578

Figs. 5 and 6 display the vulnerability indices at 12:00 noon and Node 14, respectively, selected from five scenarios. The results reveal that while Scenario 2 shows improvements in certain time periods, its vulnerability increases significantly during peak electricity consumption intervals. In contrast, Scenario 5 exhibits substantially lower grid vulnerability, with further reductions observed during peak load periods compared to other scenarios, indicating enhanced grid resilience under the proposed method.

Fig. 7 illustrates the life cycle carbon emissions of PV power generation and energy storage capacity under different scenarios. Scenario 5 exhibits to varying degrees in life-cycle carbon emissions of PV power generation compared to the other four scenarios, achieving a 44.44% reduction

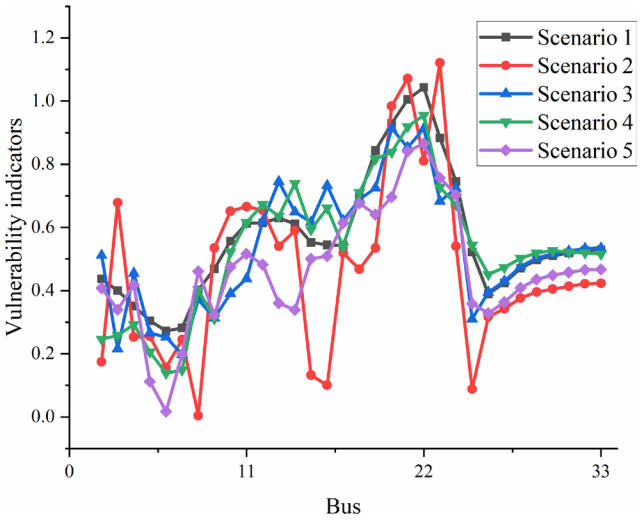

Fig. 5 Vulnerability of IEEE-33 bus at 12 noon by bus

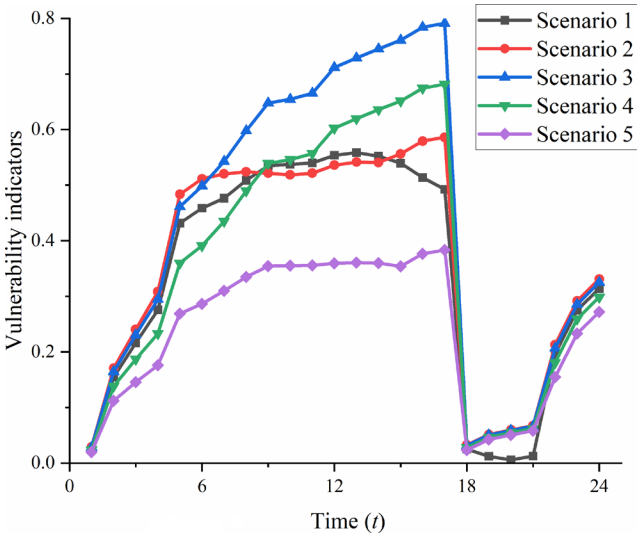

Fig. 6 24 h vulnerability of bus 14 in IEEE-33 bus

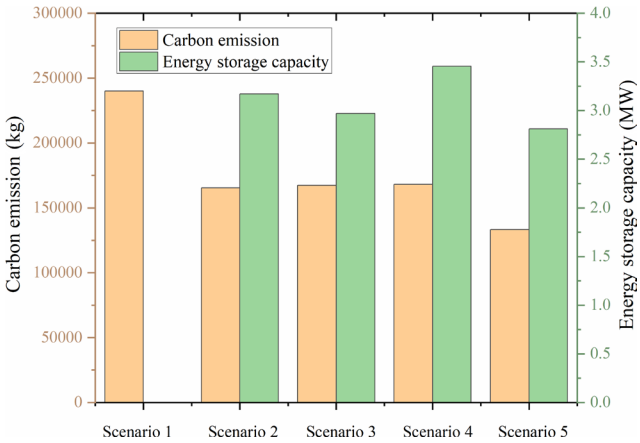

Fig. 7 Comparation of life cycle carbon emissions and energy storage capacity of PV power generation in different scenarios of IEEE-33 bus

compared to Scenario 1 and 19.36%, 20.3%, and 20.64% reductions compared to Scenarios 2, 3, and 4, respectively. Additionally, the energy storage capacity in Scenario 5 is lower than that in Scenarios 2, 3, and 4. The comprehensive analysis of life-cycle carbon emissions and energy storage capacity indicates that Scenario 5 demonstrates lower costs, leading to better economic benefits.

Fig. 8 illustrates the node voltage curves under each scenario. By comparing Scenario 1 and Scenario 2, it is evident that the introduction of an ESS significantly mitigates both voltage fluctuations and load variations in the system, demonstrating the ESS's effectiveness in suppressing voltage and load oscillations in the power grid. When comparing Scenario 5 with Scenarios 2 and 3, the results indicate that multi-objective siting and sizing of distributed PV and ESS can effectively reduce system voltage fluctuations. Furthermore, a comparison between Scenario 5 and Scenario 4 reveals that the improved non-cooperative game-driven algorithm achieves more efficient solutions.

These results demonstrate that incorporating grid vulnerability, network loss, and life-cycle carbon emissions of PV power generation as optimization objectives can improve the voltage magnitude of smart distribution grids while ensuring the economic viability of PV and ESS.

5.2 IEEE-69 distribution network system

5.2.1 Data input

To further test the scalability of the proposed method, the IEEE-69 bus distribution network system is adopted as a case study. The total grid load is 3802.1 + j2694.7 kVA, with an operational voltage of 12.66 kV. The permissible node voltage range is specified as 0.9–1.1 p.u.

5.2.2 Result analysis

In Section 4, a comparative analysis was conducted among Scenarios 1, 4, and 5 in the scenario settings. The optimization results for the IEEE-69 node system are presented in Table 3, with the siting outcomes shown in Fig. 9. As indicated in Table 3, compared to Scenario 1, Scenario 5 achieves reductions in all three objective functions: the grid vulnerability index decreased by 3.1%, network loss was reduced by 4.03%, and the life-cycle carbon emissions of PV power generation decrease by 24.92%. Additionally, compared to Scenario 4, Scenario 5 demonstrated improvements across all indicators to varying degrees.

Figs. 10 and 11 present the vulnerability indices for the three scenarios at 12:00 noon and at Node 50, respectively. As observed in Fig. 12, while Scenario 4 demonstrates partial improvements during certain time periods, its comparison with Scenario 5 highlights the effectiveness of the

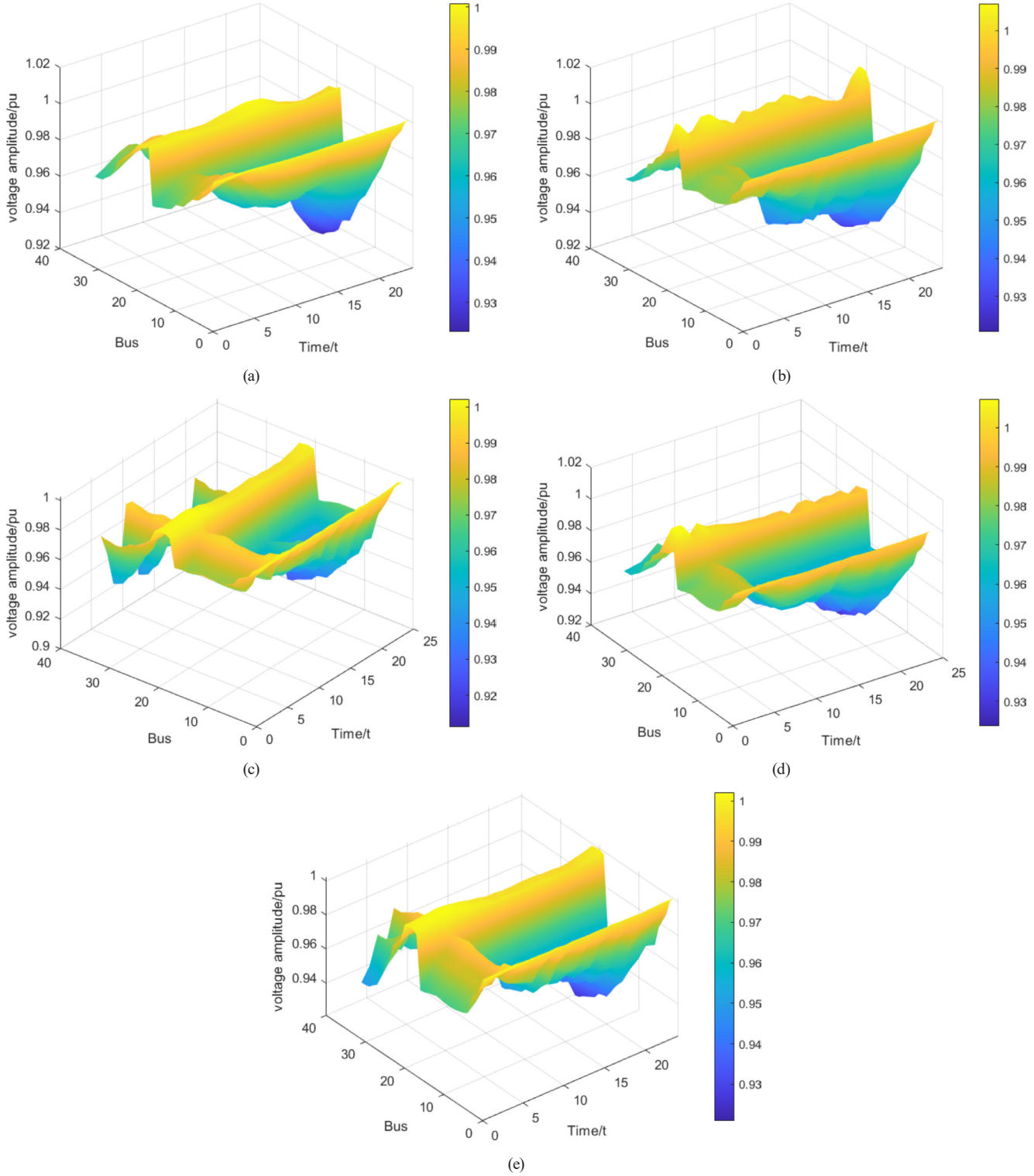

Fig. 8 Voltage at each bus for different scenarios of IEEE-69 bus: (a) Scenario 1; (b) Scenario 2; (c) Scenario 3; (d) Scenario 4; (e) Scenario 5

non-cooperative game-driven multi-objective siting and sizing method for distributed PV and ESS. The grid vulnerability in Scenario 5 is significantly lower and shows further reductions during peak load periods compared to other scenarios.

Fig. 12 shows the life cycle carbon emissions of PV generation and the total energy storage capacity under different scenarios. Scenario 5 exhibits reductions in PV life cycle carbon emissions compared to the other two scenarios. Specifically, the life cycle carbon emissions in Scenario 5

Table 3 Performance comparison of different scenario methods for IEEE-69 bus

Scenario	PV access location and capacity/MW	Energy storage access location and capacity/MW	x_1	x_2	x_3
1	50(2) 27(2)	–	0.5302	2.307	240000
4	37(2) 19(1.2243)	23(2) 65(1.8258)	0.5206	2.2861	187600
	7(1.702) 45(1.0828)	16(2) 26(1.3167)	0.52	2.2635	167090
	23(2) 35(1.4307)	15(2) 65(1.4426)	0.5226	2.2567	205840
	Average value		0.5211	2.2688	186843
5	67(1.8) 58(0.4232)	22(1.579) 21(1.8)	0.513	2.2569	133390
	60(1.3863) 2(1.8)	60(1.432) 62(1.585)	0.5169	2.1919	191180
	12(1.8) 39(1.8)	27(1.631) 19(2)	0.5112	2.1974	216000
	Average value		0.5137	2.2141	180190

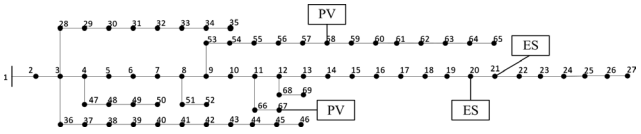

Fig. 9 IEEE-69 bus siting results

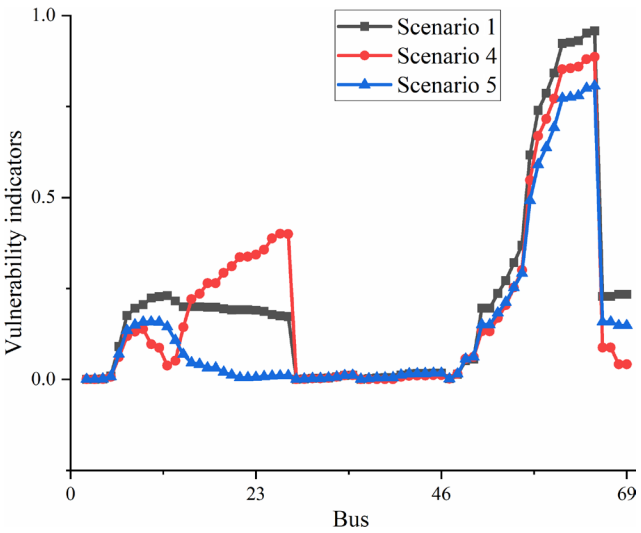

Fig. 10 Vulnerability of IEEE-69 bus at 12 noon by node

are reduced by 24.09% compared to Scenario 1 and reduced by 3.5% compared to Scenario 4. The lower energy storage capacity in Scenario 5 compared to Scenario 4 indicates better optimization effectiveness of the proposed method. Considering both life cycle carbon emissions and energy storage capacity, Scenario 5 achieves lower overall costs and demonstrates superior economic performance.

As shown in Fig. 13, the node voltage profiles under three scenarios for the IEEE-69 bus system are illustrated.

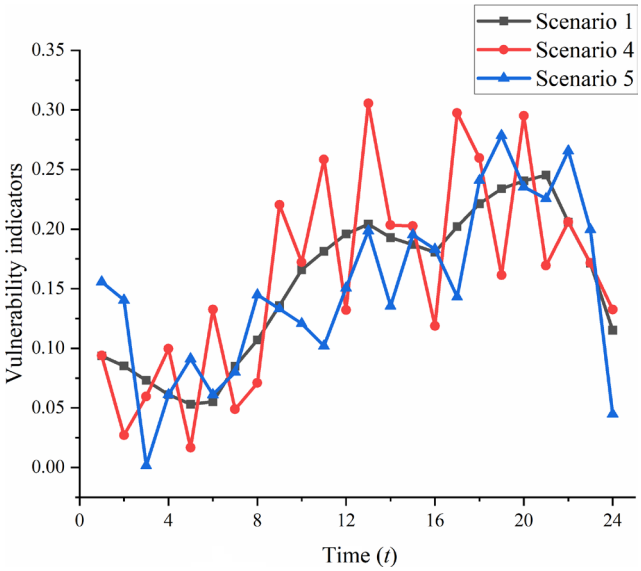

Fig. 11 24 h vulnerability of 50 of the IEEE-69 bus

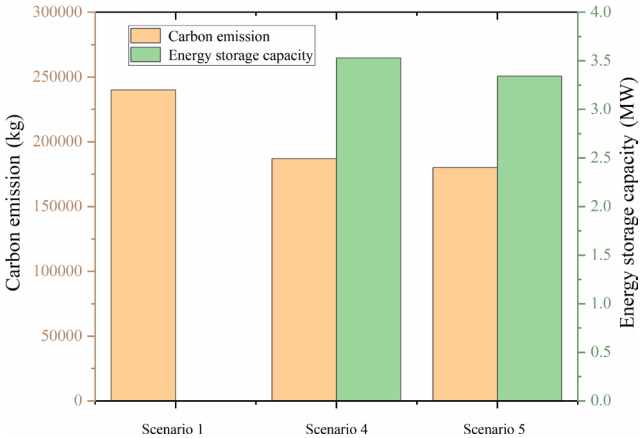

Fig. 12 IEEE-69 bus life cycle carbon emissions and energy storage

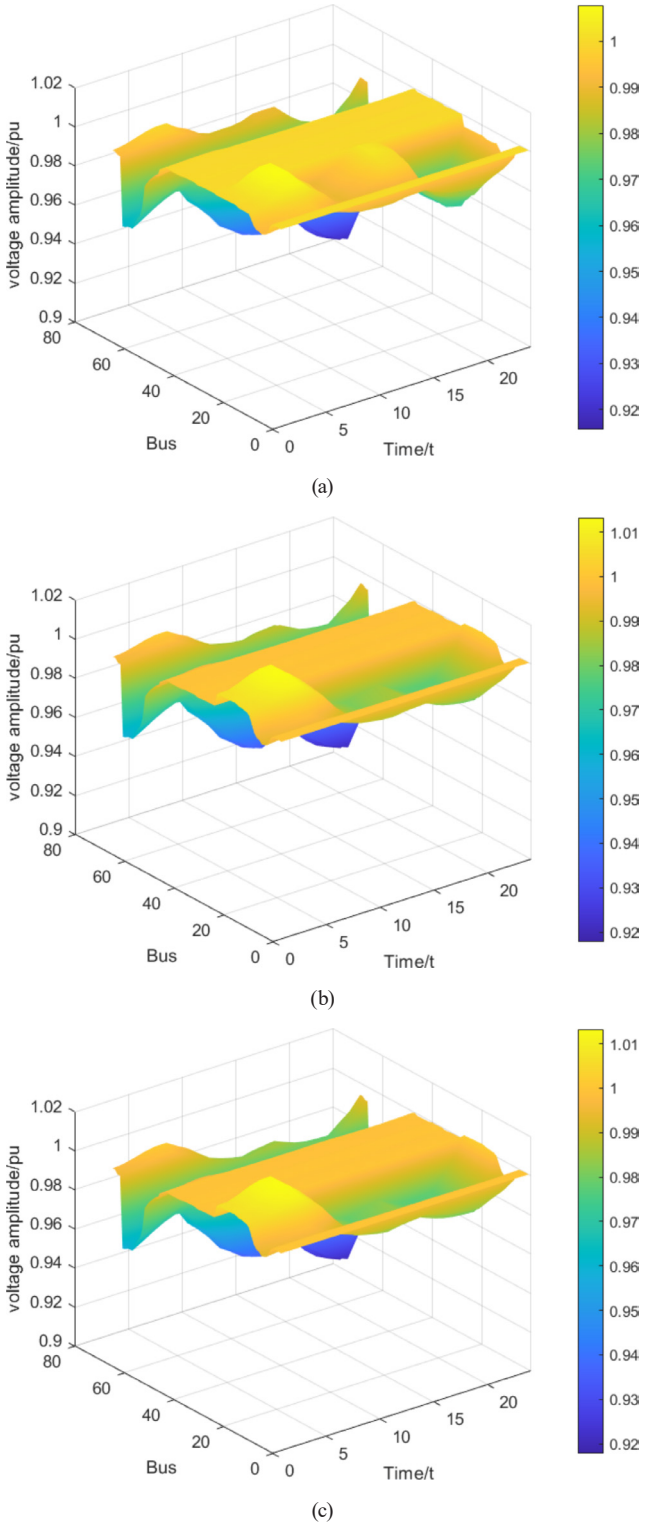

Fig. 13 Voltage amplitude at each node for different scenarios of IEEE-69 bus: (a) Scenario 1; (b) Scenario 4; (c) Scenario 5

Comparing Scenario 1 with Scenario 5, it can be observed that both voltage fluctuations and load fluctuations are significantly reduced with the integration of ESS systems, demonstrating the effectiveness of ESS in suppressing grid voltage fluctuations and load variations. Furthermore, a comparison between Scenario 5 and Scenario 4 reveals that the improved non-cooperative game-driven MOPSO algorithm effectively mitigates voltage fluctuations and load oscillations in the power grid.

5.3 Algorithm performance comparison

Section 5.3 presents a specific comparison of the performance between MOPSO and IMOPSO algorithms, using external solutions and spacing metric M for evaluation. External solutions [14] refer to the solutions in the Pareto solution set where a certain objective component is optimal during each iteration. The convergence and robustness of the algorithms can be evaluated by comparing the variation process of external solutions for a specific objective component during iterations and their values in the final generation. The metric M is used to measure the uniformity of solution distribution in the Pareto solution set, which is characterized by the mean square deviation of particle density distances in this paper.

$$M = \sqrt{\frac{1}{N}\sum_{i=e}^{N}\left[I\left(n_i\right)-\bar{I}\right]^2} \tag{26}$$

In Eq. (26), $\bar{I}$ denotes the average value of all particles $I(n_i)$ in the Pareto solution set. Both algorithms are independently run 20 times, and each iteration of either algorithm generates 20 external solutions $\left(n_i^{(k)}\right)$ corresponding to the objective (x_i). The objective values $\left(x_i\left(n_i^{(k)}\right)\right)$ associated with these external solutions are statistically analyzed, and their average values are calculated. Analyses are conducted with node vulnerability (x_1) and network loss (x_2) as the objects, and the objective values corresponding to the external solutions of the final generation are presented in Table 4. The convergence curves are shown in Fig. 14. The average values of the S metric in the final generation during the 20 runs are listed in Table 4.

As shown in the comparison of Fig. 14 and Table 4 for external solutions, the proposed method demonstrates better convergence characteristics and higher search accuracy under the non-cooperative game framework, enabled by adaptive inertia weight, crossover, and mutation

Table 4 Performance comparison of different algorithms

Algorithm	External solution		M metric
	x_1	x_2	
MOPSO	0.9001	0.2330	0.0527
Non-cooperative framework IMOPSO	0.7023	0.1235	0.0231

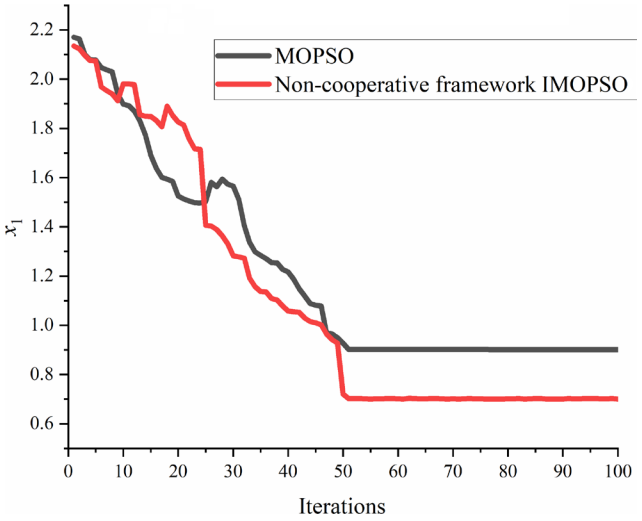

Fig. 14 Convergence curve of the external solution of Goal 1

operations. Moreover, the improved update strategy for the Pareto solution set enhances its diversity and distribution characteristics, as verified by the *M* metric in Table 4 and the results in Fig. 14.

5.4 Advantages and limitations of the study

This study demonstrates significant advantages in the field of multi-stakeholder collaborative optimization:

1. It novelly constructs a planning framework driven by non-cooperative game theory, transforming the multi-objective conflicts among power grid companies, DPV owners, and ESS operators into a Nash equilibrium problem, providing theoretical support for complex interest coordination.
2. The proposed IMOPSO algorithm exhibits high efficiency and robustness in solving high-dimensional nonlinear optimization problems, achieving dynamic balance between Pareto optimal solutions and Nash equilibrium points.
3. By integrating three objectives of grid vulnerability, network losses, and life-cycle carbon emissions of PV, it balances grid safety, economic efficiency, and low-carbon benefits. Validation in IEEE standard test [13, 15] cases shows that it reduces grid vulnerability by 2.43%, network losses by 4.29%, and carbon emissions by 44.44%, while ensuring technical feasibility through voltage quality constraints.

Despite these, the research has areas for improvement:

1. The model validation is based on idealized IEEE-33 bus and IEEE-69 bus systems, failing to fully reflect the geographical constraints and dynamic load characteristics of actual distribution networks.
2. The non-cooperative game framework assumes perfect rationality and information symmetry among participants, without considering the impacts of policies, risk preferences, etc., on decision-making behaviors.
3. The computational efficiency and convergence of the IMOPSO algorithm in ultra-large-scale distribution networks need further verification, and the parameter sensitivity is not quantitatively analyzed. The carbon emission model does not cover the full-life-cycle environmental impacts of ESSs.

Subsequent research will deeply explore the above limitations to enhance the engineering applicability and theoretical completeness of the study.

6 Conclusions

High-penetration PVs cause operational challenges due to dispersed and disordered integration. To address these issues, this study considers the tight planning-operation coupling between PV and energy storage. A non-cooperative game-driven method is proposed for optimal PV and ESS siting and sizing in smart distribution networks. The method incorporates equilibrium strategies of game participants (PV and ES units) and is solved using an improved MOPSO algorithm. Simulations are conducted on IEEE-33 bus and IEEE-69 bus distribution networks. Typical daily PV and load data are used to achieve multi-objective siting and sizing of distributed PV and ESS. The results indicate that:

1. The proposed methodology integrates three critical operational dimensions: grid vulnerability mitigation, network loss reduction, and PV life cycle carbon emissions management. This tri-objective optimization framework enhances SDN security while determining optimal distributed PV-energy storage siting-sizing configurations. The case study demonstrates that the proposed method achieves optimal locations and capacities for each distributed PV and ESS installation. It mitigates voltage vulnerability at weak nodes in smart distribution networks, reduces power losses and life cycle carbon emissions from PV generation, and decreases the distribution network's operational and maintenance costs.
2. The proposed non-cooperative game-driven equilibrium strategies under heterogeneous stakeholder frameworks are combined with an improved MOPSO algorithm to solve multi-objective optimization problems. This approach enhances convergence speed and enables effective evaluation of trade-offs between multiple objectives. As a result, it improves

the accuracy and rationality of decision-making processes. The algorithm demonstrates enhanced global optimization capability. It significantly reduces grid vulnerability, power losses, and life cycle carbon emissions from PV generation, while effectively improving the security and economic efficiency of smart distribution networks.

Building upon the proposed non-cooperative game-theoretic framework for optimal siting and sizing of DPV and energy storage (ES) systems in smart distribution networks, the subsequent research phase will conduct an in-depth exploration of planning challenges that explicitly integrate the technical and economic ramifications of stochastic PV generation. This extension aims to enhance the model's robustness by quantifying the impacts of fluctuating solar irradiance and output volatility on key performance metrics, including grid vulnerability indices, network loss profiles, and life-cycle carbon emission trajectories. Through this endeavor, the research seeks to bridge the gap between deterministic optimization paradigms and real-world operational complexities, thereby fostering a more resilient decision-making framework for sustainable distribution network planning under uncertainty.

Acknowledgements

This work was supported in part by the National Natural Science Foundation of China (No.52467008), Innovation Project for Young Science and Technology Talents in Lanzhou City (2023-QN-121), Gansu Provincial Department of Education: Youth Doctoral Support Project (2024QB-051), Key Laboratory of Modern Power System Simulation and Control·&Renewable Energy Technology (Northeast Electric Power University) Open: Fund (MPSS2025-07).

References

[1] National Energy Administration (NEA) "国家能源局举行新闻发布会　介绍前三季度可再生能源并网运行情况并解读《关于大力实施可再生能源替代行动的指导意见》" (National Energy Administration held a press conference to introduce the operation of renewable energy grid connection in the first three quarters and to explain the "Guiding Opinions on Vigorously Implementing Renewable Energy Substitution Actions)", National Energy Administration (NEA), 31 Oct., 2024. [online] Available at: https://www.nea.gov.cn/2024-10/31/c_1212406333.htm [Accessed: 26 November 2024] (in Chinese)

[2] Power Electronics and New Energy "电力电子与新能源" (Top 10 Status and Four Trends in Energy Storage), Power Electronics and New Energy, 06 May, 2024. [online] Available at: https://mp.weixin.qq.com [Accessed: 20 August 2024] (in Chinese)

[3] Zhong, H., Zhang, N., Du, E., Guo, H., Cai, Y., Wang, P., Gao, H., Li, Y., Liu, X., Kang, C., Xia, Q. "新型电力系统中的规划运营与电力市场：研究进展与科研实践" (Planning, Operation and Market of New Power System: Research Progress and Practice), Proceedings of the CSEE, 44(18, pp. 7084–7104, 2024. (in Chinese) https://doi.org/10.13334/j.0258-8013.pcsee.241076

[4] Kou, L., Zhang, Y., Ji, Y., Wu, M., Xiong, X., Hu, Z., Meng, J., Xiang, Y. "分布式储能的典型应用场景及运营模式分析" (Analysis of typical application scenarios and operation models of distributed energy storage), Power System Protection and Control, 48(4), pp. 177–187, 2020. (in Chinese) https://doi.org/10.19783/j.cnki.pspc.190447

[5] Zhou, Z., Zhang, N., Xie, X., Li, H., Kang, C. "高比例可再生能源电力系统关键技术及发展挑战" (Key technologies and developing challenges of power system with high proportion of renewable energy), Automation of Electric Power Systems, 45(9), pp. 171–191, 2021. (in Chinese) https://doi.org/10.7500/AEPS20200922001

[6] Peng, C., Chen, L., Zhang, J., Sun, H. "基于分类概率机会约束IGDT的配网储能多目标优化配置" (Multi-objective optimal allocation of energy storage in distribution network based on classified probability chance Constraint information gap decision theory), In: Proceedings of the CSEE, Nanchang, China, 2021, pp. 17–23. (in Chinese) https://doi.org/10.26914/c.cnkihy.2021.000172

[7] Zheng, Y., Song, Y., Huang, A., Hill, D. J. "Hierarchical Optimal Allocation of Battery Energy Storage Systems for Multiple Services in Distribution Systems", IEEE Transactions on Sustainable Energy, 11(3). pp. 1911–1921, 2020. https://doi.org/10.1109/TSTE.2019.2946371

[8] Li, J., Zhang, Z., Shen, B., Gao, Z., Ma, D., Yue, P., Pan, J. "The capacity allocation method of photovoltaic and energy storage hybrid system considering the whole life cycle", Journal of Cleaner Production, 275, 122902, 2020. https://doi.org/10.1016/j.jclepro.2020.122902

[9] Jiménez-Vargas, I., Rey, J. M., Osma-Pinto, G. "Sizing of hybrid microgrids considering life cycle assessment", Renewable Energy, 202, pp. 554–565, 2023. https://doi.org/10.1016/j.renene.2022.11.103

[10] Zhang, Q., Wang, D., Zhao, C., Wang, X., Ding, J., Wang, H., Zhang, X. "Low-carbon operation of smart distribution grid based on life cycle assessment and ladder-type carbon trading", Renewable Energy, 231, 120816, 2024. https://doi.org/10.1016/j.renene.2024.120816

[11] Shang, L., Wei, B., Wang, W., Xiong, X., Ci, H., Li, J., Chen, X. "主动配电网储能动态配置规划方法" (A planning method of dynamic energy storage configuration in an active distribution network), Power System Protection and Control, 48(17), pp. 84–92. (in Chinese) https://doi.org/10.19783/j.cnki.pspc.191256

[12] Li, R., Luo, P., Lin, J. "考虑有源配电网可靠性和脆弱性的储能多目标规划" (Multi-objective planning for energy storage considering the reliability and vulnerability of active distribution networks), Southern Power Grid Technology, 18(8), pp. 39–50, 2024. (in Chinese)
https://doi.org/10.13648/j.cnki.issn1674-0629.2024.08.005

[13] Yan, Q., Dong, X., Mu, J., Ma, Y. "基于改进多目标粒子群算法的有源配电网储能优化配置" (Optimal configuration of energy storage in active distribution network based on improved multi-objective particle swarm algorithm), Power System Protection and Control, 50(10), pp. 12–19, 2022. (in Chinese)
https://doi.org/10.19783/j.cnki.pspc.211106

[14] Wu, X., Liu, Z., Tian, L., Ding, D., Yang, S. "基于改进多目标粒子群算法的配电网储能选址定容" (Distribution network energy storage location and capacity determination based on improved multi-objective particle swarm algorithm), Power Grid Technology, 38(12), pp. 3405–3411, 2014. (in Chinese)
https://doi.org/10.13335/j.1000-3673.pst.2014.12.021

[15] Lu, L., Chu, G., Zhang, T., Yang, Z. "基于改进多目标粒子群算法的微电网储能优化配置" (Optimal configuration of energy storage in a microgrid based on improved multi-objective particle swarm optimization), Power System Protection and Control, 48(15), pp. 116–124, 2020. (in Chinese)
https://doi.org/10.19783/j.cnki.pspc.191172

[16] Sharma, S., Kumar, V. "A Comprehensive Review on Multi-objective Optimization Techniques: Past, Present and Future", Archives of Computational Methods in Engineering, 29(7), pp. 5605–5633, 2022.
https://doi.org/10.1007/s11831-022-09778-9

[17] Abuduwayiti, X., Lü, H., Chao, Q. "基于非合作博弈的风–光–氢微电网容量优化配置" (Capacity Optimization of Wind-Solar-Hydrogen Microgrid Based on Non-Cooperative Game Theory), Electric Power Engineering Technology, 41(2), pp. 110–118, 2022. (in Chinese)
https://doi.org/10.12158/j.2096-3203.2022.02.015

[18] Hong, L., Fan, B., Tang, C., Ge, S., Wang, Y., Guo, L. "基于博弈论的主动配电网扩展规划与光储选址定容交替优化" (Alternate optimization of active distribution network expansion planning and optical storage site selection and capacity determination based on game theory), Power System Automation, 41(23), pp. 38–45, 2017. (in Chinese)

[19] Parise, F., Grammatico, S., Gentile, B., Lygeros, J. "Distributed convergence to Nash equilibria in network and average aggregative games", Automatica, 117, 108959, 2020.
https://doi.org/10.1016/j.automatica.2020.108959

[20] Tawalbeh, M., Al-Othman, A., Kafiah, F., Abdelsalam, E., Almomani, F., Alkasrawi, M. "Environmental impacts of solar photovoltaic systems: A critical review of recent progress and future outlook", Science of The Total Environment, 759, 143528, 2021.
https://doi.org/10.1016/j.scitotenv.2020.143528

[21] Aboud, A., Rokbani, N., Fdhila, R., Qahtani, A. M., Almutiry, O., Dhahri, H., Hussain, A., Alimi, A. M. "DPb-MOPSO: A Dynamic Pareto bi-level Multi-objective Particle Swarm Optimization Algorithm", Applied Soft Computing, 129, 109622, 2022.
https://doi.org/10.1016/j.asoc.2022.109622

[22] Yan, B., Liu, W., Liu, G., Zeng, Z., Liu, Y., Cao, Y., Shi, Q., Cheng, R. "基于城市电力–地铁耦合网络的电网脆弱性评估" (Vulnerability Assessment of Urban Power Grid Based on Urban Power-Metro Coupling Network), In: Proceedings of the CSEE, Beijin,China, pp. 1–14. http://kns.cnki.net/kcms/detail/11.2107.tm.20240731.1458.002.html [Accessed: 09 April 2025] (in Chinese)

[23] Hao, X., Zhao, M., Pei, L., Li, W., Liu, Z. "基于改进Pareto算法的风/光/氢蓄储公路微电网调度决策优化" (Optimization of dispatching decision of wind/solar/hydrogen storage highway microgrid based on improved Pareto algorithm), Journal of Traffic and Transportation Engineering, 24(4), pp. 71–82, 2024.
https://doi.org/10.19818/j.cnki.1671-1637.2024.04.006